Preprint Cambridge Centre for Computational Chemical Engineering ISSN 1473 – 4273

Reactivity of Polycyclic Aromatic Hydrocarbon Soot Precursors: Kinetics and Equilibria

Angiras Menon [1,3], Jacob Martin [1,3], Jethro Akroyd [1,3], Markus Kraft [1,2,3]

released: 27 August 2020

[1] Department of Chemical Engineering
and Biotechnology
University of Cambridge
Philippa Fawcett Drive
Cambridge, CB3 0AS
United Kingdom
E-mail: mk306@cam.ac.uk

[2] School of Chemical and
Biomedical Engineering
Nanyang Technological University
62 Nanyang Drive
Singapore 637459

[3] Cambridge Centre for Advanced Research and
Education in Singapore
CREATE Tower, 1 CREATE Way
Singapore 138602

Preprint No. 258

Keywords: Cross-linking,variational transition state theory, polyaromatic hydrocarbons, reactive edge types

Edited by
Computational Modelling Group
Department of Chemical Engineering and Biotechnology
University of Cambridge
Philippa Fawcett Drive
Cambridge CB3 0AS
United Kingdom

E-Mail: c4e@cam.ac.uk
World Wide Web: http://como.ceb.cam.ac.uk/

Abstract

The thermodynamics and kinetics of cross-linking reactions between PAHs of various reactive edge types that are observed in soot precursors are explored using density functional theory. The cross-linking rate constants confirm that reactions involving aryl σ-radicals are faster than others, but rate constants for reactions between aryl σ-radicals and localised π-radicals can be as large or even larger than for two aryl σ-radicals. However, rates for all cross-linking reactions between small PAHs are likely too slow to explain soot formation. The equilibrium constants show that reactions involving σ and π-radical PAHs are the most favorable at flame temperatures. Equilibrium constants for larger PAHs show that the ability to form bonded-and-stacked structures results in enhanced equilibrium constants for the reaction of two large localised π-radicals compared to other edge types. This suggests that combined physical and chemical interactions between larger π-radical PAHs could be important in flame environments.

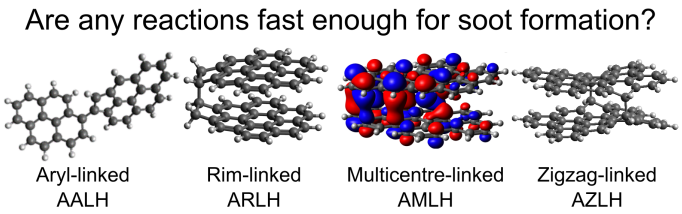

Highlights

- Cross-linking rate constants are computed for PAHs with different reactive edges.
- Reactions of σ-radicals and localised π-radicals had the largest rate constants.
- All rate constants are likely too low to explain soot nucleation.
- Equilibrium constants for cross-linking of larger PAHs show enhancement from rim bonding.
- This enhancement is dependent on the reactive edge type and is most noticeable for localised π-radicals.

Contents

1 Introduction

Soot nanoparticles are known to be a major public health concern, causing amongst other issues respiratory problems [23]. Particulate matter pollutants have also been seen to contribute to global warming on a large scale, being the second largest contributor to radiative forcing after carbon dioxide [2, 31]. However, the understanding of soot nucleation, the process by which these carbonaceous nanoparticles form in combustion processes remains unknown.

It is widely accepted that the bulk of experimental and theoretical work supports the idea that the precursors to soot formation are polycyclic aromatic hydrocarbons (PAHs) [15–17]. A variety of mechanisms have been hypothesised to attempt to explain how these PAHs interact and cluster together to form soot. This includes clustering by physical van der Waals interactions between flat PAHs [10], which several works suggest is thermodynamically unfavorable [39, 45], as well as interactions between curved PAHs and ions, which has shown to result in substantial binding energies due to the interaction between the flexoelectric dipole of curved PAHs and ions [26, 27, 29]. The interaction between ions and curved PAHs has also been seen to improve the clustering behaviour of these PAHs [3]. However, recent coupled thermodynamic-kinetic analyses of soot nucleation has suggested that purely physical processes are unlikely to produce sufficient nucleation flux for soot formation [9]. Thus mechanisms relying on reactive PAHs are often considered.

Several different types of PAHs with different reactive edges are known to exist and have been imaged in recent experimental works, such as those using high resolution atomic force microscopy (HR-AFM) [5, 40] and tunable photoionisation time of flight mass spectrometry (PI-TOF MS) [21].

The first, and perhaps most well-known of these are aryl-type σ-radicals, which are generated by abstraction of a hydrogen atom from the rim of a PAH [18, 19]. σ-radicals are known to play a central role in PAH growth in the well known hydrogen-abstraction-acetylene-addition (HACA) mechanism [10, 24, 36]. Additionally, rim-based pentagonal rings provide a double bond edge with significant reactivity [9, 48], as do curved PAHs, which have been seen to have enhanced oxidation and HACA growth rates [37, 38]. Even flat, PAHs like phenanthrene and pyrene are known to have low-aromaticity edges more prone to radical attacks [4]. Bridge forming reactions between σ-radicals and five-member ring PAHs have been studied by Violi et al. [48], who proposed the aromatic aliphatically linked hydrocarbon (AALH) mechanism. This has been expanded on more recently by Frenklach and Mebel [9]. Reactions between σ-radicals and delocalised π radicals have also been proposed by Johansson et al. [21], who suggested the clustering of hydrocarbons by radical chain reactions (CHRCR) mechanism. Where for the later, hydrogen is readily lost from the intermediate regenerating the aromatic π-radical. However, recent studies have questioned whether the collision efficiency of σ-radicals with other species are rapid enough to provide significant nucleation fluxes, without some additional effects playing a role [8, 25].

The second is the localised π-radicals, first suggested in the context of soot formation by Wang [49]. This includes diradicaloids such as acenes, which are known to have

unique localisation properties and possess near diradical nature [41]. This enables them to form multi-bridge structures [22, 49, 51]. A recent study by the authors [30], used electronic structure theory with reactivity indices to map the reactivity and bond energies of cross-links between PAHs of different edge types. Localisation of π-radicals was also demonstrated in partially saturated rim-based pentagonal rings, methylene groups, and five-member rings in PAHs. These species had been previously explored computationally by Wang [49] and Whitesides et al. [50] who both noted their stability and role in thermal rearrangements. We found that these reactive sites are able to form stable complexes that are π-stacked *and* covalently bonded. These complexes we called aromatic rim-linked hydrocarbons (ARLH). It was also shown that these localised π-radicals can be present in substantial concentrations at flame conditions [32]. Finally, multiple localised π-radical sites on a single PAH was also shown to be possible, which means a chemical polymerisation of these PAHs could be feasible as well [32].

The purpose of this work is to build on our reactivity and bond energy analysis conducted previously [30], by estimating the rate constants and equilibrium constants for cross-linking reactions between PAHs of different types. The consideration of diradicaloid species such as acenes is added and extended from this previous work as well. Density functional theory is employed in conjunction with canonical transition state theory (TST) and variational theory (VTST) to provide an initial estimate for the rate constants and equilibrium constants of these cross-linking reactions to analyse which are likely to be relevant at flame temperatures. The equilibrium constants are also computed for larger PAHs that can form ARLH complexes to get an idea of the enhancement provided by combined physical and chemical modes of complex formation.

2 Methodology

This work focuses on computing the kinetics and equilibria of reactions between PAH monomers containing different edge types. These monomers are shown in Figure 1.

The monomers include σ-radical PAHs, with A1 having the radical site on the five-member ring, and A2 having the radical site on a six-member ring. Localised π-radicals, include partially saturated rim-based pentagons, such as B1, and those with an odd number of electrons in the π-network like B2. These localised π-radicals have their spin density concentrated on a particular site. Delocalised π-radicals like C also have an odd number of π-electrons, but in contrast the electron density delocalises across the network, meaning the reactivity is also spread across the rim. Diradicaloids such as partially-embedded cyclopentaphenathrene-type molecules such as D1 and linear acenes such as pentacene (D2) have very low singlet-triplet electronic gaps, which hence impacts their reactive characteristics [41]. Monomer E, is acenaphthylene, and contains a rim-based pentagonal ring, which are known to be reactive due to the low-aromaticity five-member free edge, as well as stable and present in flames [19]. Similarly, F1 is a curved PAH, which are known to have unique properties such as substantial permanent dipole moments due to flexoelectric effects [28, 29] and enhanced reactivities [37]. Finally, phenanthrene and naphthalene, denoted F2 and F3, are well-known flat PAHs with lower aromaticity edges compared to maximally condensed benzenoid PAHs.

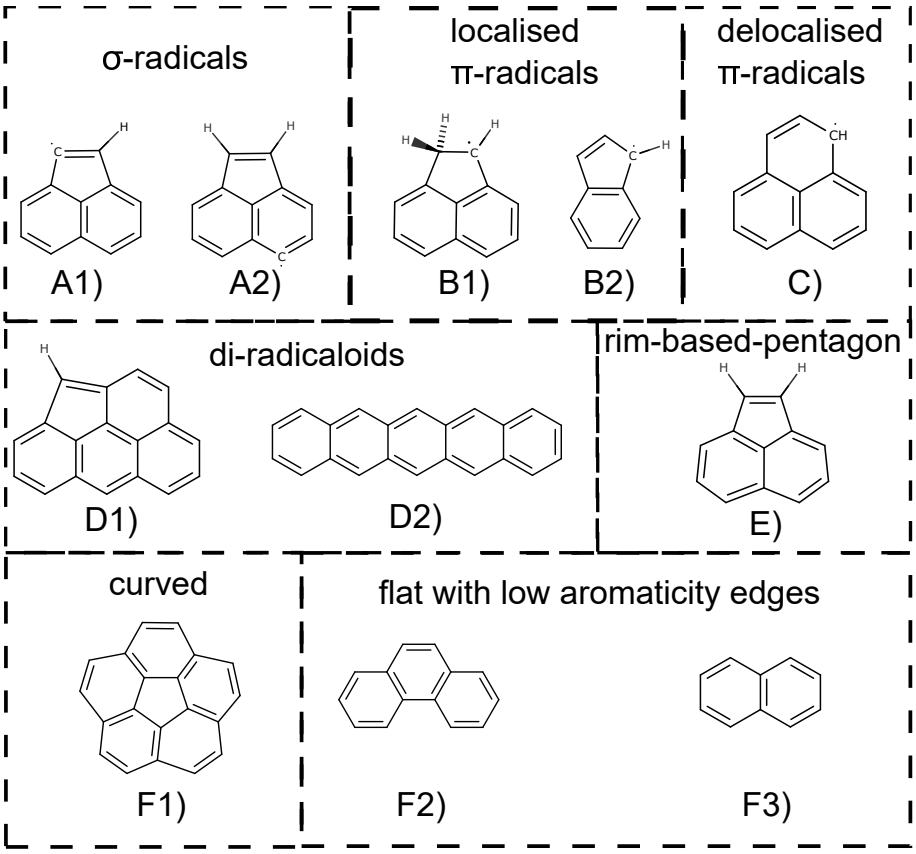

Figure 1: *PAH monomers studied in this work classified by the reactive edge type they contain.*

Geometries and frequencies in this work are derived using hybrid density functional theory (DFT) electronic structure calculations are performed at the B3LYP/6-311G(d,p) level of theory for all PAH reactants, intermediates, transition states and products. Transition states were located by means of a potential energy surface scan along the bond coordinate at the same level of theory before being optimised. Located transition states were confirmed by checking that only one imaginary frequency was present and that this vibrational mode corresponds to the reaction in question. To improve the estimate of energies of the species, single-point energy calculations were performed at the M06-2X/cc-pVTZ level of theory. This level of theory has been previously shown to describe energies and bond enthalpies for reactions between PAHs of different edge types [30], and the M06-2X functional was developed specifically to treat organic radicals, with bond enthalpies and organic barrier heights expected to be accurate to within 2 kcal/mol [18, 52]. Dispersion was included using the empirical GD3 method with M06-2X, denoted as M06-2X-D3, which is seen to estimate physical interactions to within 6 kcal/mol of high level SAPT(DFT) calculations at a fraction of the computational cost. Gaussian 16 [12] was used to perform all quantum chemical calculations.

Rate constants for the formation of cross-links between the PAH monomers of various edge types were computed using the DFT-derived molecular properties. In the case where a tight-transition state was identified, the rate was computed by canonical transition state

theory:

$$k = \frac{k_B T}{h} \frac{q^{\dagger}}{\prod_i^{n_{\text{reactants}}} q_i} \exp\left(\frac{-\Delta E_0}{RT}\right), \tag{1}$$

where k is the rate constant, k_B is the Boltzmann constant, T is temperature, h is Planck's constant, q is the total partition function, and ΔE_0 is the classical barrier height. A tunneling correction for the case of an asymmetric Eckart potential was also applied. The tight transition state rate constants were computed using Arkane as implemented in Reaction Mechanism Generator (RMG) [13].

If no transition state could be located from a potential energy surface scan, the reactions were treated as barrierless, and the rate constants were computed using angular-momentum resolved variational transition state theory as implemented in the ktools package within Multiwell [1]. Trial transition states were taken from points along the potential energy surface scan with bond separation lengths between 1.8 Å and 3.2 Å. These trial transition states had their geometries and frequencies determined at the B3LYP/6-311G(d,p) level of theory and also had their energies further refined at the M06-2X-D3/cc-PVTZ level of theory, consistent with other species and tight transition states computed in this work. The potential energy surfaces used for the VTST calculations are shown in Figure 2.

The numerical parameters for the energy and angular momentum density of states integration were taken from [1]. Namely, this involves an energy grain of 10 cm^{-1} and maximum energy of 85000 cm^{-1}, as well as an angular momentum grain of 1 cm^{-1} and maximum angular momentum of 1000 cm^{-1}.

It is worth mentioning that radical-radical reactions can require multireference methods to be modelled accurately. In this case, the PAHs studied here are large enough such that multi-reference methods would be very computationally demanding, and as such the broken symmetry approach with the unrestricted M06-2X (BS-UM06-2X) functional was chosen. Whilst this does not accurately describe the multi-configurational nature of a bond dissociation process, the broken symmetry approach and utilization of the unrestricted functional has been shown to give the correct dissociation limit, which is crucial for describing the potential energy surfaces [43]. The M06-2X functional gives good predictions of the energetics for bond dissociation, particularly among DFT methods, and should suffice for qualitative estimates of rate constants [52].

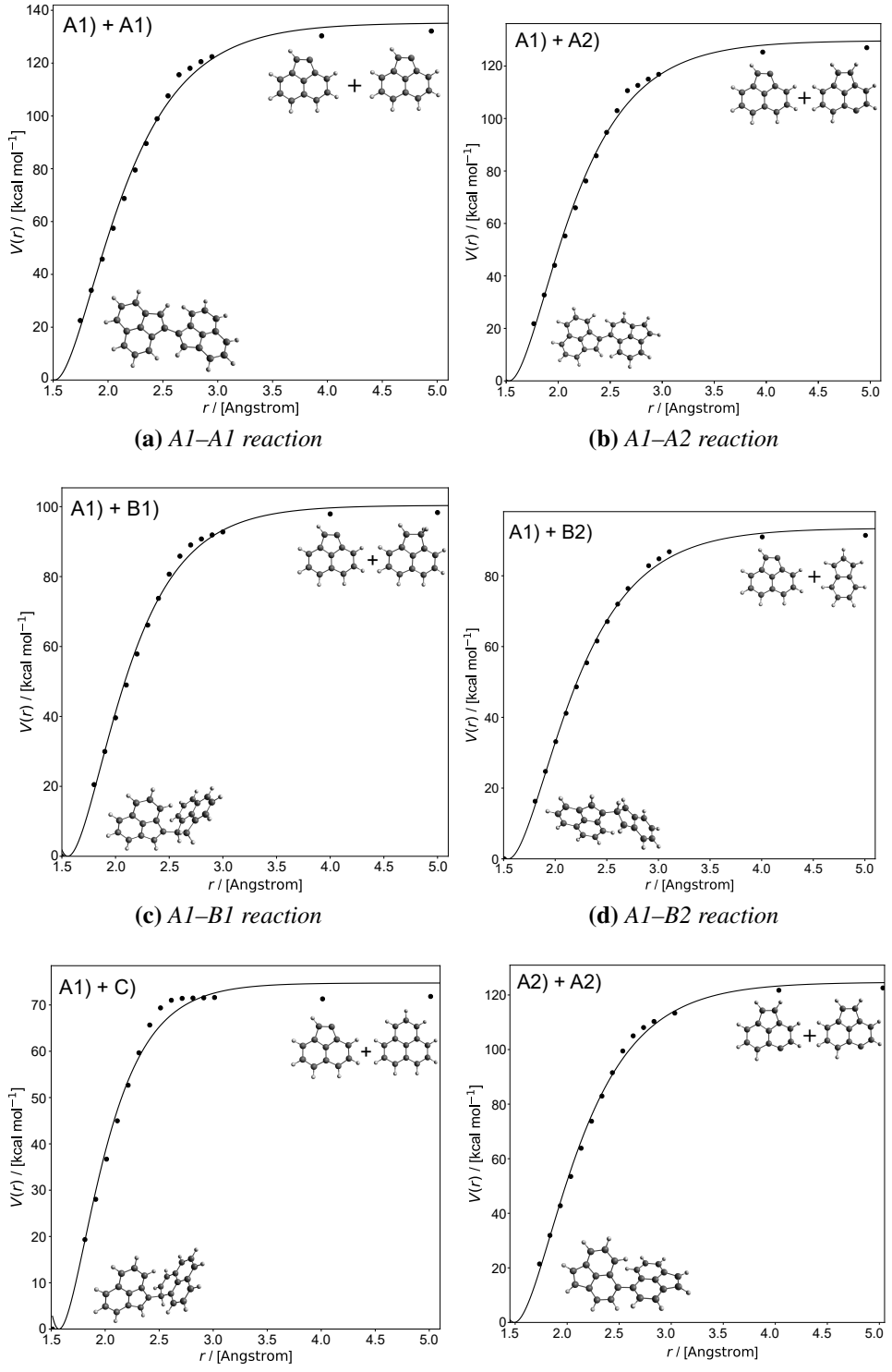

(a) *A1–A1 reaction* **(b)** *A1–A2 reaction*

(c) *A1–B1 reaction* **(d)** *A1–B2 reaction*

(e) *A1–C reaction* **(f)** *A2–A2 reaction*

Figure 2: *Potential energy surfaces for barrierless cross-linking reactions studied in this work. The energies are computed at the BS-UM06-2X/cc-PVTZ level of theory, and are fitted to a Morse potential.*

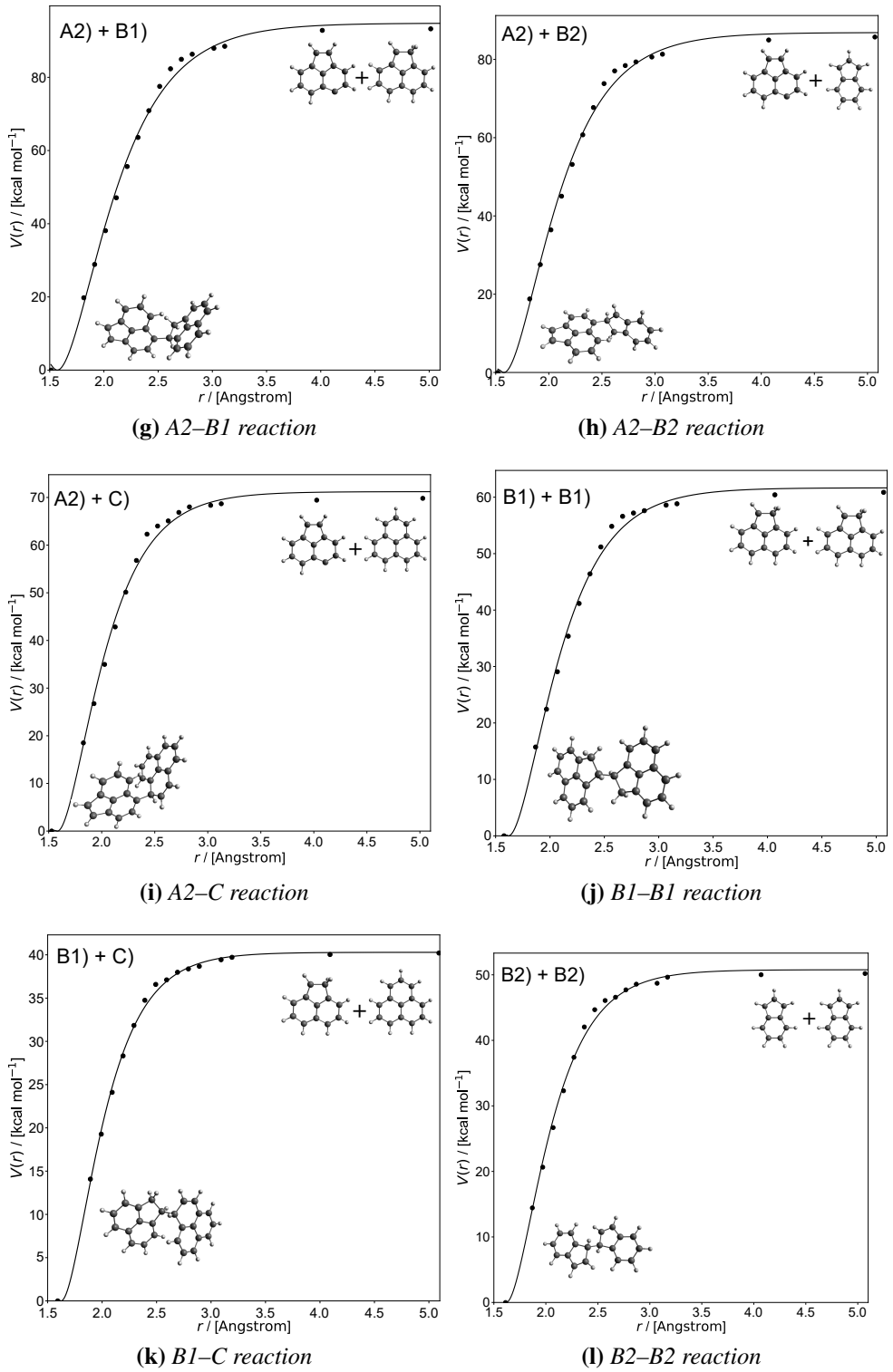

(g) *A2–B1 reaction* **(h)** *A2–B2 reaction*

(i) *A2–C reaction* **(j)** *B1–B1 reaction*

(k) *B1–C reaction* **(l)** *B2–B2 reaction*

Figure 2: *(Continued.) Potential energy surfaces for barrierless cross-linking reactions studied in this work. The energies are computed at the BS-UM06-2X/cc-PVTZ level of theory, and are fitted to a Morse potential.*

As a test of the method, the rate constant for the recombination of phenyl radicals to produce biphenyl was computed using the methodology described above. This rate constant has been predicted theoretically by Tranter et al. [46], who employed the multireference CASPT2(2e,2o) method as well as the cc-pVDZ basis set to model the interaction energy, along with variable reaction coordinate transition state theory (VRC-TST). A very recent high temperature shock tube study by Jin et al. [20] also estimated the rate constant for phenyl radical recombination. These are used for comparison in Figure 3.

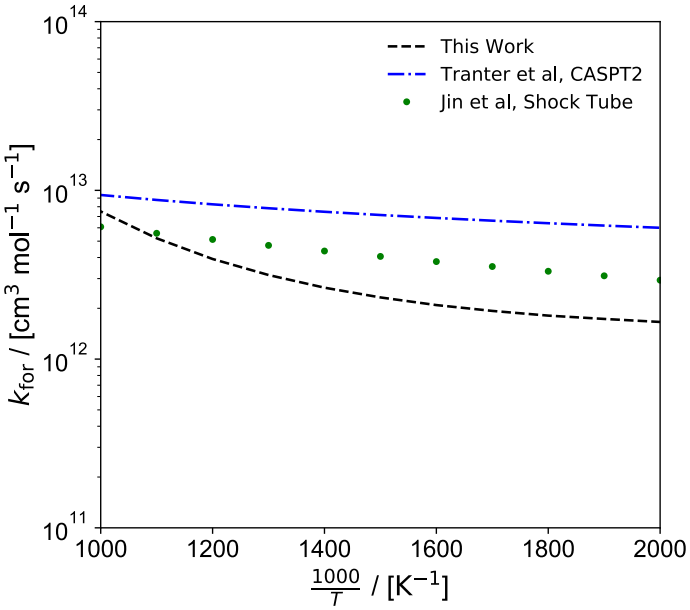

Figure 3: *Comparison of the rate constant of phenyl radical recombination estimated using BS-UM06-2X/cc-pVTZ and VTST to those estimated by Tranter et al. [46] and Jin et al. [20].*

Figure 3 suggests reasonable agreement between the rate constant for phenyl radical recombination computed using the methodology employed in this work and the predictions of Tranter et al. [46] and Jin et al. [20] in the range of 1000–2000 K. The negative temperature dependence and order of magnitude predicted are captured by the use of BS-UM06-2X/cc-pVTZ and VTST, although the decrease in rate constant is steeper in comparison. This is likely due to the less accurate interaction energy predicted by the DFT method used here compared to the multireference methods employed by Tranter et al. [46], as well as differences in the prediction of the enthalpy of reaction for the recombination, which is predicted to be -119.1 kcal/mol by BS-UM06-2X/cc-pVTZ compared to -117.9 predicted by CASPT2(2e,2o)/cc-pVDZ. Nevertheless, this comparison does suggest that the methodology here should suffice for initial estimates of the rate constants of radical-radical PAH reactions.

Additionally, several of the cross-linking reactions also possessed barriers below 2 kcal/mol, which is near the expected uncertainty in barrier height predictions with M06-2X. This means that these cross-linking reactions could actually have submerged barriers. However, as a tight transition state was found and confirmed, canonical transition state theory was still deemed appropriate to use to derive initial estimates of rate constants for these processes, but further refinement is likely necessary.

3 Results and Discussion

3.1 Bond energies and classification of cross-links

Figure 4 presents an updated version of the matrix of bond energies presented in Martin et al. [30]. The matrix has been updated to include an acene-type PAH, namely pentacene, which are known to possess diradical character [33]. Indenyl has also been reclassified to a localised-π radical, due to its spin mainly being concentrated on a single rim atom on the five-member ring. We also found that for the σ-radicals and indenyl the central pentagonal carbon atom was more reactive than the site given by the Clar analysis (see Fig 2**h**), which is corrected from our previous work [30]. Additionally, the type of cross-link has been classified and named by the type of radical or edge type that initiates the bond-forming reaction. For example, the reactions initiated by the σ-radicals A1 and A2 result in aromatic aryl-linked hydrocarbons (AALH), and reactions initiated by the localised-π radical are termed aromatic rim-linked hydrocarbons (ARLH), in reference to the bonding at the rim as well as stacking that is only possible for localised π-radicals. Reactions between delocalised π-radicals and the diradicaloids result in multi-centre bonds, or pancake bonds, due to several different possible orientation centres, and are denoted as aromatic multicentre-linked hydrocarbons (AMLH). Finally, diradicaloids bonding along their zig-zag edges are given the acronym AZLH, but these reactions are observed to be symmetry forbidden in practice and so did not have rates computed due to their low bond energies.

In general, the bond energies decrease in strength from the aryl σ-radical type edges seen in A down to the low aromaticity edge types seen in F. Consequently, AALH species

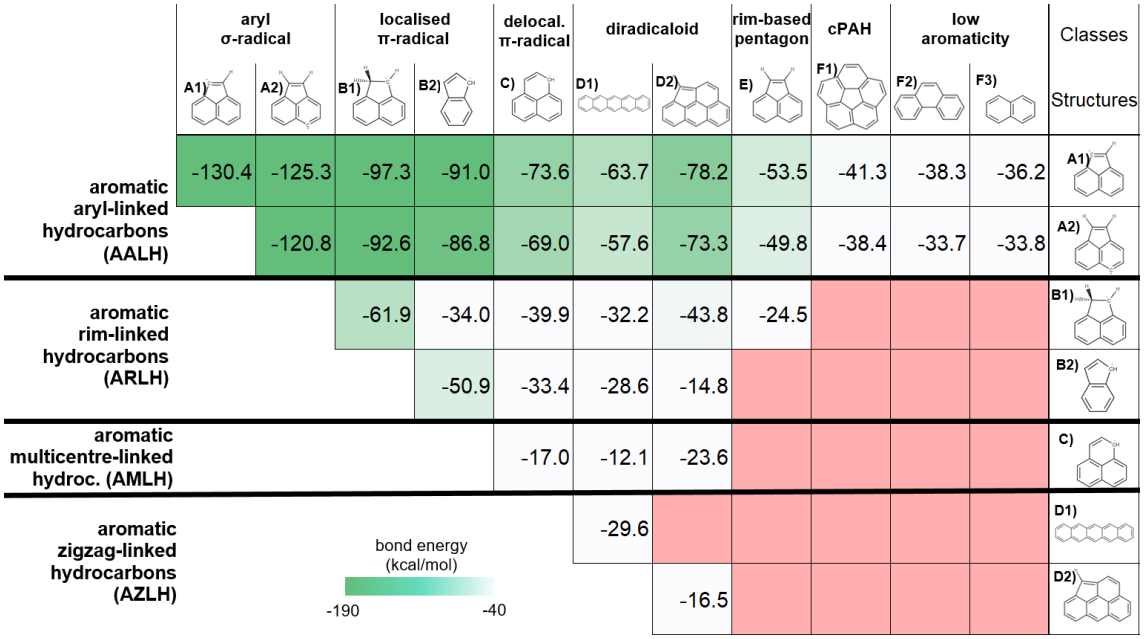

Figure 4: *Bond energies of cross-linking between PAHs of different edge types computed at the M06-2X-D3/cc-pVTZ level of theory.*

are much more likely to form bonds stable at flame temperatures, followed by ARLH and AMLH. Of note is the diradicaloid D2. This partially-embedded pentagon edge type generally forms stronger than expected bonds with the aryls as well as the localised and delocalised π-radical structures B1 and C, when compared to other π-radical and diradicaloids B2, C, and D1.

3.2 Barrier Heights

In subsequent discussions, the reactions can be separated into reactions with and without barriers. The barrierless reactions include the reactions of the aryl σ-radicals with any other PAH with a radical edge-type, that is A1 and A2 reacting with any PAH with edge type A, B, or C, reactions of localised π-radical B1 with itself and delocalised π-radical C, as well as the reaction between indenyl(B2) and itself. As is expected, the barrierless reactions are generally those between radicals of different types that result in high bond energies. All other cross-linking reactions were seen to have barriers, in that a transition state for the reaction was located. These barriers are provided in Table 1:

Table 1: *Predicted barrier heights for formation of cross-links between PAHs at the M06-2X-D3/cc-pVTZ level of theory.*

Reaction	Barrier Height / kcal mol^{-1}
A1 + D1 → A1D1	1.29
A1 + D2 → A1D2	1.12
A1 + E → A1E	0.55
A1 + F1 → A1F1	0.76
A1 + F2 → A1F2	1.63
A1 + F3 → A1F3	2.77
A2 + D1 → A2D1	1.22
A2 + D2 → A2D2	0.45
A2 + E → A2E	1.27
A2 + F1 → A2F1	1.63
A2 + F2 → A2F2	2.61
A2 + F3 → A2F3	3.20
B1 + B2→ B1B2	4.11
B1 + D1 → B1D1	1.67
B1 + D1 → B1D1b	1.44
B1 + D2 → B1D2	2.10
B1 + E → B1E	5.35
B2 + C → B2C	2.51
B2 + D1 → B2D1	1.26
B2 + D2 → B2D2	15.37
C + C → CC	9.88
C + D1 → CD1	4.03
C + D2 → CD2	8.51

It is known that barrier heights for a family of reactions tend to have a linear relationship between the barrier height and the enthalpy of reaction. Figure 5 presents a plot of the barrier heights of the various cross-linking reactions against their bond enthalpy, a Brønsted-Evans-Polanyi (BEP) type plot for the reactions with barriers.

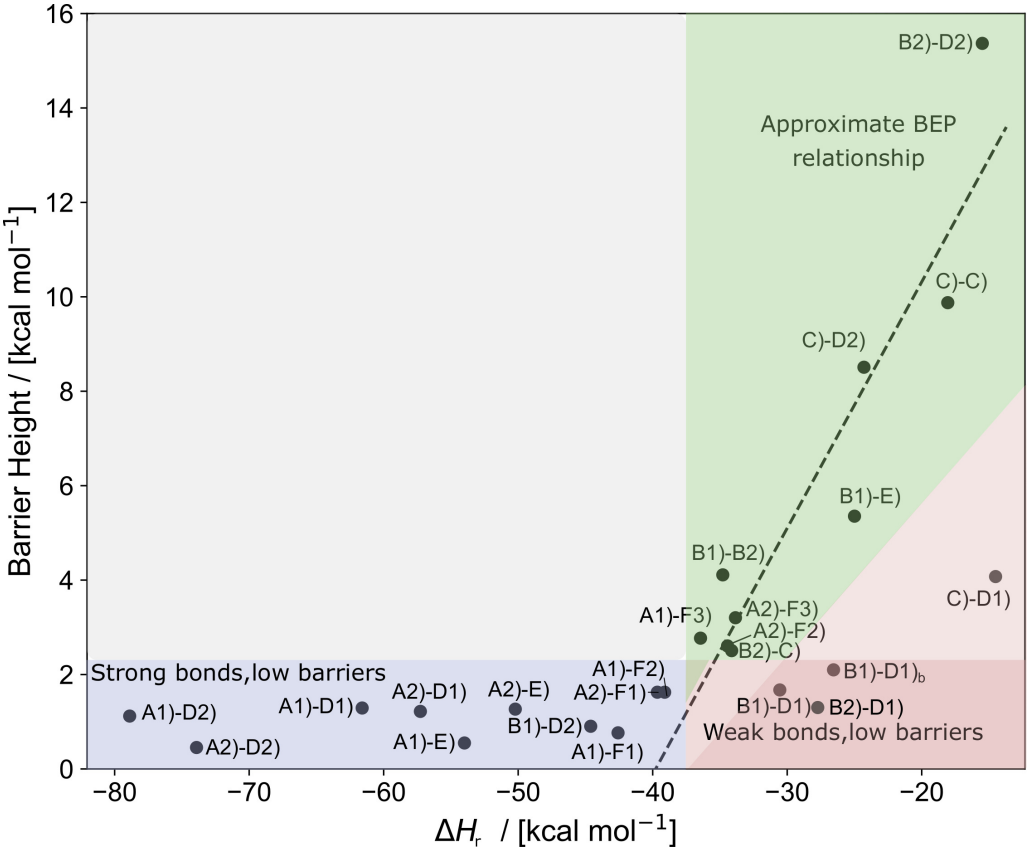

Figure 5: *Full BEP plot of the barrier heights against bond enthalpy for the various cross-linking reactions*

Three regions can be identified. Firstly, for weaker bonds with an enthalpy less than $\sim$40 kcal/mol and barriers greater than approximately 2 kcal/mol, an approximate BEP relationship can be seen, where the relationship between the classical barrier height and bond enthalpy is roughly linear. Cross-linking reactions occurring in this regime include reactions involving the delocalised π-radical C with other edge types, reactions of localised π-radical edge type B with all non-diradicaloid edge types, namely B, C and E, and reactions of the aryl σ-radical edge types A with the low aromaticity edges of standard planar PAHs F2 and F3. The delocalised π-radical C is generally seen to have high barriers for its cross-linking reactions. This is most likely due to its aromatic stabilisation, which also results in delocalised electron density and lower reactivity, hence the higher barriers. Other high barrier-low bond enthalpy reactions include the reactions between B2 and D2, as well as B1 and E. Both of these reactions involve a cross-link forming between two carbon atoms in five-member rings, with the two carbons forming the bond also being bonded to a hydrogen as well. This would suggest that bonds between five-member rings are likely less favorable unless there is sufficient radical character among the reacting PAHs.

The next region seen on the plot are also cross-linking reactions that have low bond enthalpies, but whose classical threshold energies for the reaction are much lower than is expected if a BEP relationship is followed. The reactions in this regime all involve the diradicaloid pentacene or D1 reacting with the various π-radicals of edge type B and C. This would suggest that although the bonds formed are weak, it is quite facile to do so. Diradicaloids are known to have near radical character, and acenes like D1 are known to have increasing degrees of diradical character with increasing size from Clar analyses [42]. This results in increasing reactivity around the central rings of such acenes. In the case of D2, the strongest cross-links with B1, B2, and C all formed on the central ring, in line with the Clar analyses of the diradical [41]. This would suggest that the diradicaloid nature of the acenes contributes to their barriers being much lower than what would be expected solely from the bond enthalpies.

The third and final region is for cross-links with bond enthalpies greater than 40 kcal/mol and classical barriers lower than 2 kcal/mol. As mentioned previously, the uncertainty in M06-2X is around the 2 kcal/mol as well, and so the predicted barriers in this region must be viewed with caution. The cross-links present in this region are the majority of those involving the aryl radical edge type A, which is not surprising given their high bond enthalpies. Reactions between edge type A and the curved PAH edge type F1 can be seen to have lower expected barriers in contrast to the low aromaticity flat edge type of PAHs F2 and F3. In addition, most cross-linking reactions involving A1 have lower predicted barriers than than those involving A2, suggesting that the aryl σ-radical on a rim five-member ring is more reactive than on a six-member ring These predictions are in agreement with previous studies that suggest curved PAHs and five-member rings possess higher reactivity [37, 50] than counterpart flat PAHs and six-member rings. Notably, the only cross-link not involving a PAH with edge type A is the one between B1 and D2. As noted above, D2 forms stronger cross-links than expected, and this is reflected in the low barriers for the cross-linking reaction. This once again suggests that diradicaloids containing five-member rings are substantially more reactive than other types of closed-shell PAHs.

3.3 Rate Constants

Figure 6 presents the Arrhenius plots for the forward rate constants for forming cross-links between PAHs with different reactive edge types.

The forward rate constants for the reactions with barriers are all concave in nature, which is the expected behaviour for most rate constants, with the phenomenological activation energies increasing with temperature. Looking at the rate constants, at the higher temperature range of interest to flames (1500–2000 K), the rate constants span four orders of magnitude, from approximately 10^8 $cm^3mol^{-1}s^{-1}$ for the reactions with the highest threshold energies, to 10^{12} $cm^3mol^{-1}s^{-1}$ for the cross-linking reactions in the strong bond-low barrier regime in the BEP plot. Of note are the rate constants for the reactions of A1 and A2 with the diradicaloid D2 as well as the reaction between A1 and rim-based pentagon E. These reactions have very low barriers and yet are estimated to be of the same order of magnitude as the barrierless combination reactions across the temperature range of 300–2000 K. These rate constants are of the order of the abstraction and acetylene addition

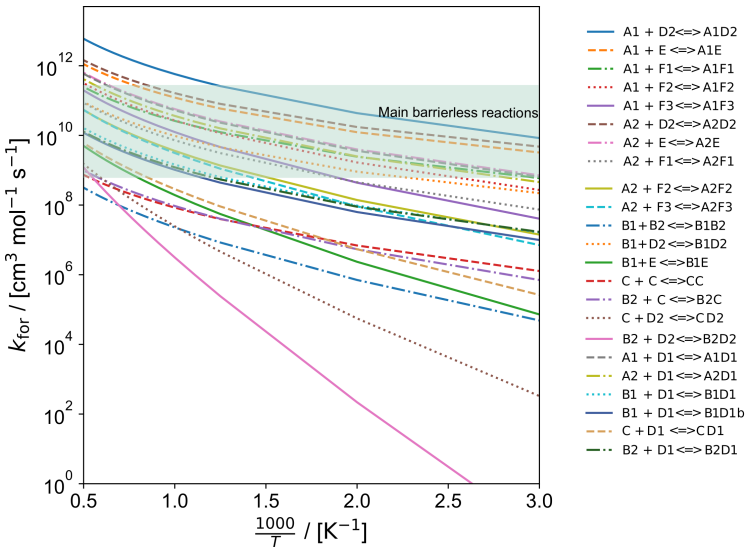

(a) *Cross-link reactions with Barriers*

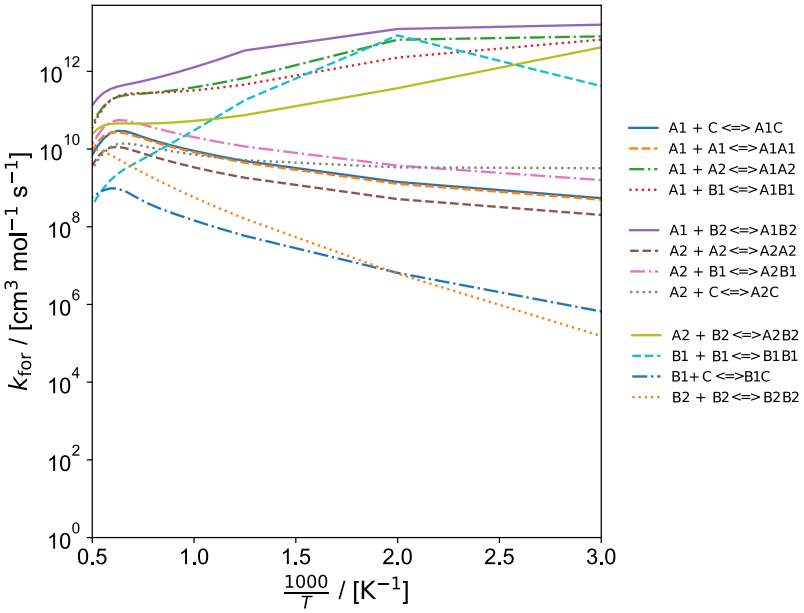

(b) *Cross-link reactions without Barriers*

Figure 6: *Arrhenius plots for the forward rate constants of forming a cross-linking between PAHs with different reactive edge types.*

steps in the well known hydrogen-abstraction-acetylene-addition (HACA) PAH growth mechanism [11].

In the case of the barrierless reactions, at the temperature range of 1500–2000 K, the rate constants are in a similar range, from approximately 10^8 cm^{3}mol^{-1}s^{-1} for the reactions with the lowest bond energies between localised π-radical B and delocalised π-radical C, to slightly below 10^{12} cm^{3}mol^{-1}s^{-1} for the higher bond energies between reactive edge types A and B. It can also be seen that the barrierless reactions between two indenyls or B2 and between B1 and C1, are lower in magnitude and more temperature dependent. In

contrast, the reactions between A1 and A2, A1 and B1, A1 and B2, and A2 and B2 are higher in magnitude. The other reactions involving the aryl σ-radicals are also weakly temperature dependent, which is commonly observed for barrierless reactions [14].

The rate constants for all of the barrierless reactions do show regions of negative temperature dependence. This negative temperature dependence tends to manifest either at higher temperatures of around 1600–1700 K for the reactions which are below 10^{11} $cm^3mol^{-1}s^{-1}$ in magnitude. Similar behaviours were observed for the rate constants computed using VRC-TST and CASPT2 interaction energies for combination channels involving phenyl and propargyl radicals [35]. In the case of the reaction between two B1 monomers, A1 and B2, A2 and B2, A1 and B1, and A1 and A2, the negative temperature dependence is observed for the bulk of the temperature range. Persistent negative temperature dependence is usually attributed to high-energy collisional effects limiting the flux through the dividing surface, and has also been observed for recombination reactions between phenyl and allyl reactions [34, 35].

Additionally, Figure 6b also shows that the radical-combination rate constants involving species A1 are larger than for the counterpart reactions involving species A2. This again suggests that the reactivity of the aryl σ-radical is higher for a radical site on a rim five-member ring than a six-member ring. However, it is worth noting that the largest rate constant for the aryl-aryl reactions is that between A1 and A2, which is one of the fastest reactions in the temperature range and is much faster than two A1 monomers or two A2 monomers reaction. This highlights the potential significance of reactions between radical sites on five and six-member ring species.

The Arrhenius plot also highlights the potential importance of localised π radical species. This is exemplified in the fact that the rate constants for the reactions between A1 and the localised π-radicals B1 and B2 are some of the largest, with the reaction between A1 and B2 being even faster than the reaction between A1 and A2. The next predicted fastest reactions in the flame temperature range of 1500–2000 K are all again reactions between a σ-radical and a localised π-radicals, namely the reactions between A1 and B1, A2 and B2, and A2 and B1. This suggests that reactions between σ-radicals and localised π-radicals are possible and may indeed be important. Finally, the rate constant between two B1 monomers, that is the localised π-radical can also be observed to have a substantially large rate constant at lower temperatures, where it is noticeably much faster than any other re-combination reaction between two identical PAHs. The B1-B1 reaction is competitive with reactions between A1 and B2, A1 and A2, and A1 and B1 until 800 K, and could be important in this range. At 1000 K, the combination of two B1 monomers appears to be competitive with reactions between A2 and localised π-radicals. It was previously seen that at these lower temperatures, the localised π-radicals on a rim five-member ring are expected to be in higher concentrations than the σ-radical A1, and so the B1-B1 reaction may play a role. Even at the lower flame temperature ranges of 1400–1500 K, the rate constant is competitive with the combination reactions of A2 with A2, A1 and C, and B2 as well as the reaction between two B2 molecules. At temperatures above this, this reaction is substantially slower. This ability of the partially saturated rim five-member rings to react suggest that the formation of PAHs with bridge bonds between pentagons, or penta-linked PAHs, is important at lower temperatures, but is substantially less important at higher temperatures.

In the case of the reactions with barriers, the forward and reverse rate constants have been fitted to the modified Arrhenius expression:

$$k = AT^n \exp\left(\frac{-E_a}{RT}\right) \tag{2}$$

In the case of barrierless reactions, the forward rate constants required a sum of two modified Arrhenius expressions to achieve a suitable fitting. The reverse cross-link breaking reactions in this case could be suitably fitted to a single modified Arrhenius expression. The rate constants for these reactions are presented in Table 2.

Table 2: *Arrhenius fittings for the rate constants for the cross-linking between PAHs possessing different reactive edge types. Rates are computed at the M06-2X/cc-pVTZ//B3LYP/6-311G(d,p) level of theory. The units are cm, kcal, mol, K, and s.*

Reaction	A_1	n_1	$E_{A,1}$	A_2	n_2	$E_{A,2}$
			With Barrier			
A1 + D1 → A1D1	49.46	3.09	1.08			
A1D1 → A1 + D1	1.62×10^{13}	0.56	61.59			
A1 + D2 → A1D2	860.41	3.01	0.98			
A1D2 → A1 + D2	2.80×10^{14}	0.56	78.54			
A1 + E → A1E	86.62	3.07	0.32			
A1E → A1 + E	8.06×10^{13}	0.43	53.63			
A1 + F1 → A1F1	19.87	3.07	0.47			
A1F1 → A1 + F1	2.15×10^{13}	0.40	42.37			
A1 + F2 → A1F2	25.43	3.10	1.26			
A1F2 → A1 + F2	1.95×10^{13}	0.46	39.67			
A1 + F3 → A1F3	17.35	3.12	2.35			
A1F3 → A1 + F3	1.63×10^{13}	0.43	38.27			

Continued on next page.

Continued from previous page.

Reaction	A_1	n_1	$E_{A,1}$	A_2	n_2	$E_{A,2}$
A2 + D1 → A2D1	20.06	3.16	0.97			
A2D1 → A2 + D1	1.51×10^{12}	0.64	57.04			
A2 + D2 → A2D2	135.21	3.04	0.26			
A2D2 → A2 + D2	7.93×10^{13}	0.60	72.76			
A2 + E → A2E	52.50	3.09	1.05			
A2E → A2 + E	8.66×10^{13}	0.46	50.34			
A2 + F1 → A2F1	5.42	3.13	1.21			
A2F1 → A2 + F1	9.78×10^{12}	0.45	40.21			
A2 + F2 → A2F2	4.82	3.12	2.17			
A2F2 → A2 + F2	5.30×10^{12}	0.48	35.86			
A2 + F3 → A2F3	4.80	3.13	2.69			
A2F3 → A2 + F3	8.81×10^{12}	0.44	35.98			
B1 + B2→ B1B2	2.43	2.57	3.36			
B1B2 → B1 + B2	1.80×10^{11}	0.59	35.01			
B1 + D1 → B1D1	1.90	3.05	1.20			
B1D1 → B1 + D1	3.46×10^{11}	0.85	29.42			
B1 + D1 → B1D1b	1.44	3.05	1.35			
B1D1b → B1 + D1	2.54×10^{11}	0.78	26.14			
B1 + D2 → B1D2	8.85	3.05	0.50			
B1D2 → B1 + D2	9.49×10^{11}	0.90	29.42			
B1 + E → B1E	1.78	3.02	4.62			
B1E → B1 + E	4.37×10^{11}	0.68	27.94			
B2 + C → B2C	2.64	2.66	2.01			
B2C → B2 + C	2.77×10^{11}	0.70	32.96			
B2 + D1 → B2D1	1.50	3.04	0.99			
B2D1 → B2 + D1	5.44×10^{11}	0.68	27.62			
B2 + D2 → B2D2	0.34	3.37	14.39			
B2D2 → B2 + D2	1.78×10^{11}	0.87	28.79			

Continued on next page.

Continued from previous page.

Reaction	A_1	n_1	$E_{A,1}$	A_2	n_2	$E_{A,2}$
C + C → CC	2.02	2.64	5.62			
CC → C + C	5.61×10^{11}	0.54	16.53			
C + D1 → CD1	1.17	3.06	3.67			
CD1 → C + D1	7.69×10^{11}	0.58	15.43			
C + D2 → CD2	0.62	3.10	7.84			
CD2 → C + D2	2.60×10^{11}	0.71	30.65			
		Barrierless				
A1 + A1 → A1A1	2.33×10^{1}	2.83	-0.24	6.26×10^{4}	2.65	26.26
A1A1 → A1 + A1	1.85×10^{21}	-1.76	134.98			
A1 + A2 → A1A2	2.71×10^{14}	-1.05	-1.76	20.31	4.00	31.69
A1A2 → A1 + A2	1.44×10^{31}	-4.65	126.98			
A1 + B1 → A1B1	1.81×10^{10}	0.21	-3.09	2.09×10^{61}	-12.55	79.16
A1B1 → A1 + B1	7.34×10^{26}	-3.51	97.80			
A1 + B2 → A1B2	7.15×10^{24}	-4.03	2.01	1.61×10^{21}	-3.59	-0.85
A1B2 → A1 + B2	1.82×10^{33}	-5.31	92.95			
A1 + C → A1C	4.25×10^{4}	2.33	1.71	3.09×10^{4}	2.38	1.88
A1C → A1 + C	2.25×10^{20}	-1.64	76.77			
A2 + A2 → A2A2	7.91	2.86	-0.26	2.14×10^{21}	-1.92	42.84
A2A2 → A2 + A2	6.71×10^{20}	-1.74	124.90			
A2 + B1 → A2B1	1.01×10^{3}	2.45	-0.07	2.11×10^{21}	-2.19	37.14
A2B1 → A2 + B1	5.03×10^{23}	-2.40	97.39			
A2 + B2 → A2B2	16.47	2.68	-7.17	2.08×10^{21}	-2.70	17.30
A2B2 → A2 + B2	8.60×10^{16}	-0.76	81.22			
A2 + C → A2C	932.05	2.20	-1.53	2.14×10^{21}	-2.18	34.72
A2C → A2 + C	5.40×10^{23}	-2.77	72.12			
B1 + B1 → B1B1	5.50×10^{23}	-4.14	-0.98	1.34×10^{23}	-3.97	-1.23
B1B1 → B1 + B1	1.29×10^{-53}	-11.91	72.32			
B1 + C → B1C	2.16×10^{-1}	3.12	2.07	2.37×10^{36}	-6.32	56.99
B1C → B1 + C	4.50×10^{17}	-1.05	46.57			
B2 + B2 → B2B2	1.46×10^{2}	2.62	5.95	2.42×10^{36}	-5.54	76.25
B2B2 → B2 + B2	4.01×10^{14}	0.27	58.35			

3.4 Equilibrium Constants

Whilst the forward rate constants for several of the reactions between different edge types were seen to be of the order of 10^{11} and 10^{12} $cm^3mol^{-1}s^{-1}$ at flame temperatures, it is known that reversibility is particularly important in soot nucleation [7, 47]. Previous works on physical dimerization between small PAHs such as pyrene have similarly fast forward rate constants, but is known to be highly reversible at flame temperatures and thus unfavorable [44, 49]. To get an idea of reversibility and favorability at flame temperatures of these cross-linking reactions, the equilibrium constant can be computed. This is presented in

Figure 7.

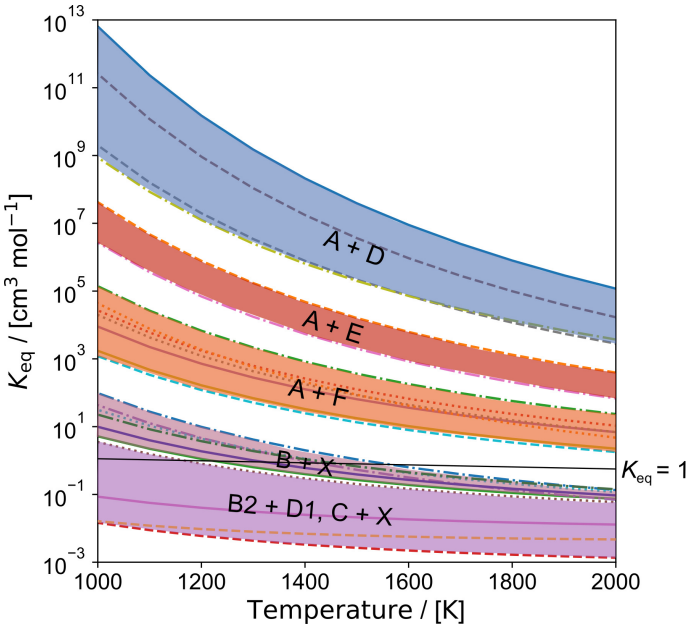

(a) *Cross-link reactions with Barriers*

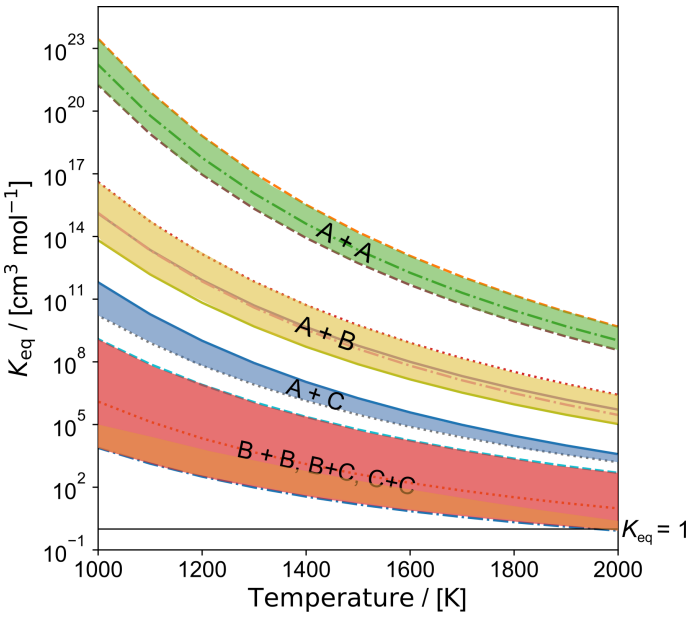

(b) *Cross-link reactions without Barriers*

Figure 7: *Equilibrium constants for forming a cross-link between PAHs with different reactive edge types.*

Figure 7 shows that the equilibrium constants do group by the reactive edge types involved, which is represented by the shaded bands in the plot. The magnitude of the equilibrium constants also mostly reflect the bond energies of the cross-link, which is expected as this is the enthalpic contribution to the equilibrium constant. The largest equilibrium constants are seen for the reactions containing the aryl σ-radical edge type A, followed by

reactions between these radicals and the localised π-radicals B as a consequence. Most of the cross-linking reactions here have equilibrium constants well above 1 at flame temperatures, and thus have low reversibility as a result. The exceptions to this are the reactions involving edge types B and C with edge types C, D, and E that also have a barrier to reaction. These are seen to be quite reversible at flame temperatures. Several, but not all, of these reactions do have correspondingly low bond energies.

However, there are clear entropic contributions to the equilibrium constant as well, which is reflected in the fact that the reactions between A1 or A2 and B2 have equilibrium constants that are one to several orders of magnitude greater than those between edge types A and D, despite the fact that the bond energy for B2 with A1 and A2 is noticeably lower than that for D2 with A1 and A2. The equilibrium constant for two B2 PAHs forming a cross-link is also greater than those for reactions between edge types A and E. Additionally, the equilibrium constant for two B1 monomers reacting is also slightly larger than those between edge types A and D, again despite the lower bond energies. Likewise, the reaction between the π-radicals B1 and C has an equilibrium constant substantially higher than those between B1 and D1 or D2, as well as between B2 and B1 and B2 and C, even though the bond energies are rather similar. The equilibrium constant for the reaction between two C molecules is also comparable to those between edge types A and F, despite the C–C bond energy being substantially weaker, again suggesting the importance of the entropic contributions, as well as highlighting the favorable nature of reactions involving π-radicals that are not necessarily reflected in simply the bond energies.

3.5 Enhancement due to Bonding and Stacking

The equilibrium constants show that cross-linking between certain reactive edge types on PAHs form very stable bonds which are much less likely to be reversible. However, a previous study on bridge-forming reaction kinetics between acepyrene (edge type E) and pyrenyl (edge type A), found that even with a forward rate constant of the order of 10^{12} $cm^3mol^{-1}s^{-1}$, the process was insufficient to generate the required nucleation flux for soot formation [9]. Another previous work of dimerization of two pyrene σ-radicals (edge type A) using reactive molecular dynamics, showed collision efficiencies of 0.001 significantly lower than the 0.01–1.0 values required in simulations [25]. Given reactions with type-A edges possess the highest forward rates this suggests insufficient rates are found for all reactions explored for small PAH soot formation.

Our previous suggestion to provide such an enhancement was that larger localised-π radical species are able to both bond and stack in rim-bonds, that is they can condense through physical interactions and subsequently chemically cross-link, which is something that aryl σ-radicals are unable to achieve [30]. We initially showed this with the additive stabilisation effect of intermolecular interactions on top of the covalent bonding for a variety of rim-linked PAHs [30].

To further explore the potential enhancement effect of bonding and stacking, the equilibrium constant was calculated for larger PAHs containing the different reactive edge types that can bond and stack (B,C,D and E). These larger PAHs were all chosen to have similar molecular weight, roughly in the range of 420-430 Da, compared to 150-160 Da

for monomers B,C, and E. It is worth noting that the M06-2X-D3 does overestimate the physical interactions by roughly 6 kcal/mol compared to SAPT(DFT) results, suggesting again that the comparison between sites is the focus of this section [30]. This is seen in Figure 8.

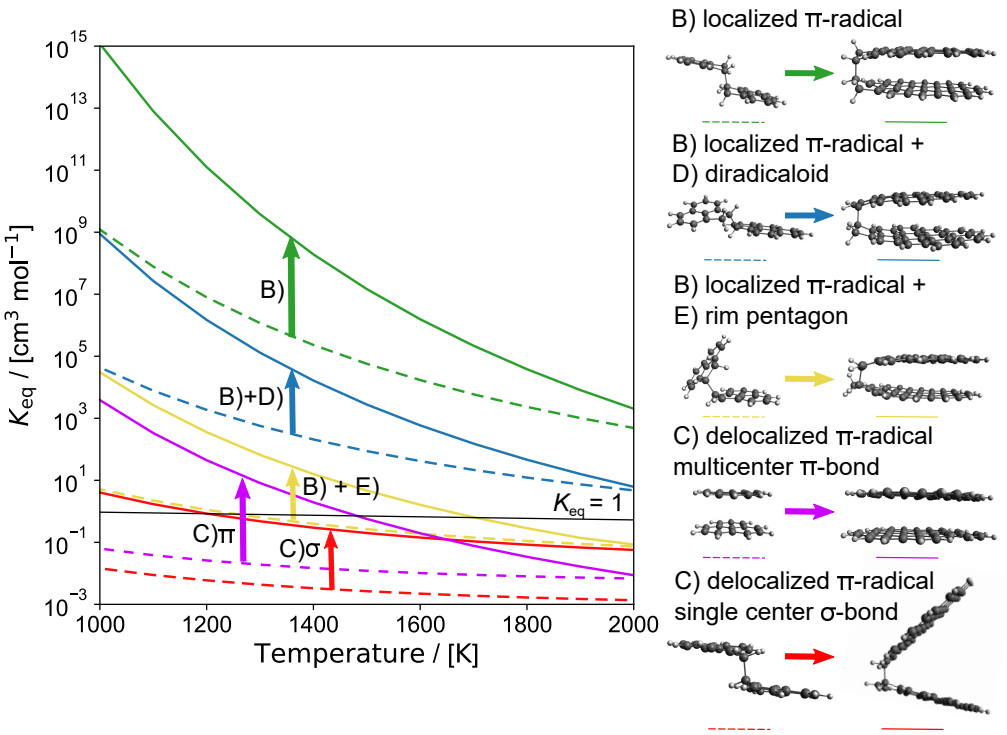

Figure 8: *Equilibrium constants for cross-linking reactions between larger PAH reactions that can result in bonded and stacked structures. The dashed lines represent the equilibrium constant for smaller PAHs with the same reactive edge types, and the arrows represent the enhancement effect.*

Figure 8 shows that there are substantial increases in the equilibrium constant for the larger PAHs compared with the smaller PAHs discussed so far. It is clear that the degree of enhancement is dependent on the type of reactive edges and the type of bond and stacking configuration. The enhancement in equilibrium constant is largest for a rim-linked structure between two localised π-radicals of edge type B, followed by edge type B and D, and finally edge type B and E. The dispersion enhancements for B and D and B and E are only slightly less than for a stacked, multi-centre π-bond between two larger delocalised π-radicals of edge type C. Overall, the increase in equilibrium constant is one to two orders of magnitude larger for a rim-bonded structure of two localised π-radicals edge types compared to the increases for other edge types.

It is worth noting that whilst the delocalised π-radical C can also form a σ-bond (otherwise known as a σ-dimerisation), the resulting structure does not stack, and the contribution of dispersion interactions is significantly lower than for reactions involving a localised π-radical (justifying our new naming as rim-linked). As a consequence, this reaction has the smallest enhancement effect, but this enhancement effect is more consistent across the 1000–2000 K range. Nevertheless, dimerisation of a larger delocalised π-radical like C is

most likely still unfavorable at temperatures above 1500 K. In contrast, even though the enhancement wanes at higher temperatures, the bond and stack effect does mean that at this same temperature of 1500 K, the reaction between larger PAHs of edge type B and E is still favorable, which was not the case for smaller PAHs with these edge types. The effect is still most promising for reactions between two localised π-radical PAHs, which was also seen to have rate constants rivaling reactions between aryl σ-radicals in edge type A.

The estimation here is also likely to be a lower bound, as the effect of first forming a physically bound PAH dimer followed by a subsequent rim-bond formation on the thermodynamics and kinetics has not been considered and could be enhanced further by internal rotors as recently suggested by Frenklach and Mebel [9]. They argued that rotationally excited collisions could enhance the stability and frequency of such bridge forming reactions, resulting in a substantial increase in the nucleation flux. A possible way in which such an enhancement could occur is due to physical interactions between PAHs before internal rotation and subsequent rim-bond formation. However, determining how much these effects will enhance collision efficiencies and reaction rates between the PAHs would likely require molecular dynamics and is the topic of further work.

Another enhancement could occur from having multiple localised π-radical sites on a single PAH containing multiple rim pentagonal rings. We have previously shown that an appreciable fraction of such PAHs can form diradicals in the flame as hydrogen is added and abstracted from these sites [32]. More sites per molecules would allow for more opportunities to bond after physical condensation. This could also allow for a chain reaction to proceed.

All in all, the preliminary results here do suggest that the combined chemical and physical aggregation between localised π-radical PAHs is quite favorable at flame temperatures, and whether or not this provide a route to forming larger clusters of PAHs and ultimately soot warrants further investigation.

4 Conclusions

In this work, the thermodynamics and kinetics of cross-linking reaction between PAHs possessing different reactive edge types has been studied by means of density functional theory calculations. Computations of the bond energies and barrier heights generally affirmed that cross-linking reactions that resulted in the formation of strong bonds generally had low barriers. This was primarily the case for reactions involving PAHs with edge type A, or aryl-type σ-radicals. One noticeable exception was for reactions between localised-π radicals, or edge type B, and acene diradicaloids, or edge type D1. These reactions were seen to have very low barriers, despite forming weak bonds. Additionally, reactions involving two PAH radicals were broadly barrierless, namely reactions between two PAHs of types A (aryl σ-radicals), B (localised-π radicals), and C (delocalised-π radicals).

The computation of the forward rate constants confirmed that reactions involving edge type A are faster than others. It was noted that generally having the σ-radical on the five-member ring resulted in faster kinetics than when the σ-radical was on the six-member

ring. At flame temperatures of 1400–2000 K, the forward rate constants were generally of the order of 10^8 $cm^3mol^{-1}s^{-1}$ to 10^{12} $cm^3mol^{-1}s^{-1}$. Notably, the rate constants between PAHs with edge type A and edge type D and edge type A and edge type B were seen to be as large or even larger than for that between two of edge type A. It was also seen that the rate constant for the reaction between A1 and A2 was substantially faster than between A1 and A1 or A2 and A2. The reaction between two localised π-radicals on rim five-member rings was seen to be notably faster at temperatures below 1000 K, but then declines and is one of the slowest reactions at 2000 K. Reactions involving combinations of edge types B, C, D, and E were generally seen to be slower in comparison. Generally, all computed rate constants are unlikely to be high enough to result in substantial enough fluxes for processes such as soot formation on their own, including suggestions involving cross-links on five-member rings [6] and delocalised π-radicals PAHs [21].

Analysis of the equilibrium constants showed most of these cross-linking reactions have substantial equilibrium constants and stability at flame temperatures, provided they involved one PAH of edge type A, or two PAHs with radical edge types A, B, or C. The localised π-radicals were seen to have large equilibrium constants for reactions with edge types A, B, and C, and were seen to be more reactive than all edge types aside from type A. It was also noted that despite having large forward rate constants in some cases, reactions of PAHs with diradicaloid edge type D were seen to have lower equilibrium constants than those involving edge types A, B, and C, highlighting their relative reversibility.

Computations of the equilibrium constants for larger PAHs that are able to bond and stack in rim-bonds showed that there is a substantial enhancement in the equilibrium constant that is dependent on the PAH edge types. It was observed that a larger enhancement was present for reactions between two localised-π radicals PAHs of edge type B than for other edge types that could bond and stack, which highlights the difference in dispersion interactions between different edge types. This suggests that these dispersion effects could potentially promote reactions of larger localised π-radicals. These effects could be further enhanced by considering the role of dynamics such as internal rotors and multiple localised π-radical sites on the same aromatic species. Further work is necessary to study the dynamics of reactions and combined physical and chemical interactions involving these localised π-radicals to determine if such reactions are able to provide the nucleation flux required to explain soot formation.

Acknowledgements

This research is supported by the National Research Foundation, Prime Minister's Office, Singapore under its under its Campus for Research Excellence and Technological Enterprise (CREATE) programme. AM gratefully acknowledges Johnson Matthey for financial support. MK gratefully acknowledges the support of the Alexander von Humboldt foundation.

Supplementary Data

The Gaussian log files for all optimised PAHs, transition states, and trial transition states for the barrierless reactions are provided via the University of Cambridge data repository (https://doi.org/10.17863/CAM.56771) and can also be provided upon request.

References

[1] J. Barker, T. Nguyen, J. Stanton, C. Aieta, M. Ceotto, F. Gabas, T. Kumar, C. Li, L. Lohr, A. Maranzana, et al. Multiwell-2017 software suite. *Ann Arbor, Michigan*, 2017.

[2] T. C. Bond, S. J. Doherty, D. W. Fahey, P. M. Forster, T. Berntsen, B. J. Deangelo, M. G. Flanner, S. Ghan, B. Kärcher, D. Koch, et al. Bounding the role of black carbon in the climate system: A scientific assessment. *J. Geophys. Res.:Atmospheres*, 118(11):5380–5552, 2013. doi:10.1002/jgrd.50171.

[3] K. Bowal, J. W. Martin, A. J. Misquitta, and M. Kraft. Ion-induced soot nucleation using a new potential for curved aromatics. *Combustion Science and Technology*, 191(5-6):747–765, 2019. doi:10.1080/00102202.2019.1565496.

[4] E. Clar, B. McAndrew, and M. Zander. The establishment of double bond character in methyl derivatives of phenanthrene, pyrene, chrysene and coronene by NMR. *Tetrahedron*, 23(2):985–993, 1967. doi:10.1016/0040-4020(67)85046-4.

[5] M. Commodo, K. Kaiser, G. De Falco, P. Minutolo, F. Schulz, A. D'Anna, and L. Gross. On the early stages of soot formation: Molecular structure elucidation by high-resolution atomic force microscopy. *Combustion and Flame*, 205:154–164, 2019. doi:10.1016/j.combustflame.2019.03.042.

[6] A. D'Anna, A. Violi, A. D'Alessio, and A. F. Sarofim. A reaction pathway for nanoparticle formation in rich premixed flames. *Combustion and Flame*, 127(1): 1995–2003, 2001. doi:10.1016/S0010-2180(01)00303-0.

[7] N. Eaves, S. Dworkin, and M. Thomson. The importance of reversibility in modeling soot nucleation and condensation processes. *Proceedings of the Combustion Institute*, 35(2):1787–1794, 2015. doi:10.1016/j.proci.2014.05.036.

[8] M. Frenklach. New form for reduced modeling of soot oxidation: Accounting for multi-site kinetics and surface reactivity. *Combustion and Flame*, 201:148 – 159, 2019. ISSN 0010-2180. doi:https://doi.org/10.1016/j.combustflame.2018.12.023.

[9] M. Frenklach and A. M. Mebel. On the mechanism of soot nucleation. *Physical Chemistry Chemical Physics*, 22(9):5314–5331, 2020. doi:10.1039/D0CP00116C.

[10] M. Frenklach and H. Wang. Detailed modeling of soot particle nucleation and growth. *Symposium (International) on Combustion*, 23(1):1559–1566, 1991. doi:10.1016/S0082-0784(06)80426-1.

[11] M. Frenklach, R. I. Singh, and A. M. Mebel. On the low-temperature limit of HACA. *Proceedings of the Combustion Institute*, 37(1):969–976, 2019. doi:10.1016/j.proci.2018.05.068.

[12] M. Frisch, G. Trucks, H. Schlegel, G. Scuseria, M. Robb, J. Cheeseman, G. Scalmani, V. Barone, G. Petersson, H. Nakatsuji, et al. Gaussian 16. *Revision A*, 3, 2016. Gaussian Inc. Wallingford CT 2016.

[13] C. W. Gao, J. W. Allen, W. H. Green, and R. H. West. Reaction Mechanism Generator: Automatic construction of chemical kinetic mechanisms. *Computer Physics Communications*, 203:212–225, 2016. doi:doi.org/10.1016/j.cpc.2016.02.013.

[14] L. B. Harding, Y. Georgievskii, and S. J. Klippenstein. Predictive theory for hydrogen atom- hydrocarbon radical association kinetics. *The Journal of Physical Chemistry A*, 109(21):4646–4656, 2005. doi:10.1021/jp0508608.

[15] B. S. Haynes and H. G. Wagner. Soot formation. *Progress in Energy and Combustion Science*, 7(4):229–273, 1981. doi:10.1016/0360-1285(81)90001-0.

[16] K. Homann and H. G. Wagner. Chemistry of carbon formation in flames. *Proceedings of the Royal Society of London. Series A. Mathematical and Physical Sciences*, 307(1489):141–152, 1968.

[17] K. H. Homann and H. G. Wagner. Some new aspects of the mechanism of carbon formation in premixed flames. In *Symposium (International) on Combustion*, volume 11, pages 371–379. Elsevier, 1967.

[18] D. Hou and X. You. Reaction kinetics of hydrogen abstraction from polycyclic aromatic hydrocarbons by H atoms. *Physical Chemistry Chemical Physics*, 19(45): 30772–30780, 2017. doi:10.1039/C7CP04964A.

[19] J. B. Howard. Carbon addition and oxidation reactions in heterogeneous combustion and soot formation. *Symposium (International) on Combustion*, 23(1):1107 – 1127, 1991. ISSN 0082-0784. doi:https://doi.org/10.1016/S0082-0784(06)80371-1. Twenty-Third Symposium (International) on Combustion.

[20] H. Jin, B. R. Giri, D. Liu, and A. Farooq. A high temperature shock tube study of phenyl recombination reaction using laser absorption spectroscopy. *Proceedings of the Combustion Institute*, 2020. doi:10.1016/j.proci.2020.06.164.

[21] K. Johansson, M. Head-Gordon, P. Schrader, K. Wilson, and H. Michelsen. Resonance-stabilized hydrocarbon-radical chain reactions may explain soot inception and growth. *Science*, 361(6406):997–1000, 2018. doi:10.1126/science.aat3417.

[22] D. Koley, E. Arunan, and S. Ramakrishnan. Computational investigations on covalent dimerization/oligomerization of polyacenes: Is it relevant to soot formation? *Journal of Computational Chemistry*, 33(21):1762–1772, 2012. doi:10.1002/jcc.23014.

[23] P. J. Landrigan, R. Fuller, N. J. R. Acosta, O. Adeyi, R. Arnold, N. N. Basu, A. B. Baldé, R. Bertollini, S. Bose-O'Reilly, J. I. Boufford, P. N. Breysse, T. Chiles, et al. The Lancet Commission on pollution and health. *The Lancet*, oct 2017. ISSN 01406736. doi:10.1016/S0140-6736(17)32345-0.

[24] M. Liu and W. H. Green. Capturing aromaticity in automatic mechanism generation software. *Proc. Combust. Inst.*, 37(1):575–581, 2019. doi:10.1016/j.proci.2018.06.006.

[25] Q. Mao, D. Hou, K. H. Luo, and X. You. Dimerization of polycyclic aromatic hydrocarbon molecules and radicals under flame conditions. *J. Phys. Chem A.*, 122 (44):8701–8708, 2018. doi:10.1021/acs.jpca.8b07102.

[26] J. Martin, R. Slavchov, E. Yapp, J. Akroyd, S. Mosbach, and M. Kraft. The polarization of polycyclic aromatic hydrocarbons curved by pentagon incorporation: The role of the flexoelectric dipole. *J. Phys. Chem. C.*, 0(ja), 2017. doi:10.1021/acs.jpcc.7b09044.

[27] J. W. Martin. Polar curved polycyclic aromatic hydrocarbons in soot formation. *Proceedings of the Combustion Institute*, 37(1):1117 – 1123, 2019. ISSN 1540-7489. doi:https://doi.org/10.1016/j.proci.2018.05.046.

[28] J. W. Martin, G. J. McIntosh, R. Arul, R. N. Oosterbeek, M. Kraft, and T. Söhnel. Giant fullerene formation through thermal treatment of fullerene soot. *Carbon*, 125: 132–138, 2017. doi:10.1016/j.carbon.2017.09.045.

[29] J. W. Martin, M. Botero, R. I. Slavchov, K. Bowal, J. Akroyd, S. Mosbach, and M. Kraft. Flexoelectricity and the formation of carbon nanoparticles in flames. *The Journal of Physical Chemistry C*, 122(38):22210–22215, 2018. doi:10.1021/acs.jpcc.8b08264.

[30] J. W. Martin, D. Hou, A. Menon, L. Pascazio, J. Akroyd, X. You, and M. Kraft. Reactivity of polycyclic aromatic hydrocarbon soot precursors: Implications of localized π-radicals on rim-based pentagonal rings. *The Journal of Physical Chemistry C*, 123(43):26673–26682, 2019. doi:10.1021/acs.jpcc.9b07558.

[31] J. R. McConnell, R. Edwards, G. L. Kok, M. G. Flanner, C. S. Zender, E. S. Saltzman, J. R. Banta, D. R. Pasteris, M. M. Carter, and J. D. W. Kahl. 20th-Century Industrial Black Carbon Emissions Altered Arctic Climate Forcing. *Science*, 317 (5843):1381–1384, 2007. doi:10.1126/science.1144856.

[32] A. Menon, J. Martin, G. León, D. Hou, L. Pascazio, X. You, and M. Kraft. Reactive localized π-radicals on rim-based pentagonal rings: properties and concentration in flames. *Proceedings of the Combustion Institute*. In Press.

[33] T. Minami, S. Ito, and M. Nakano. Fundamental of diradical-character-based molecular design for singlet fission. *The Journal of Physical Chemistry Letters*, 4(13): 2133–2137, 2013. doi:10.1021/jz400931b.

[34] A. N. Morozov and A. M. Mebel. Theoretical study of the reaction mechanism and kinetics of the phenyl+ allyl and related benzyl+ vinyl associations. *The Journal of Physical Chemistry A*, 123(9):1720–1729, 2019. doi:10.1021/acs.jpca.9b00345.

[35] A. N. Morozov and A. M. Mebel. Theoretical study of the reaction mechanism and kinetics of the phenyl+ propargyl association. *Physical Chemistry Chemical Physics*, 22(13):6868–6880, 2020. doi:10.1039/D0CP00306A.

[36] D. S. N. Parker, R. I. Kaiser, T. P. Troy, and M. Ahmed. Hydrogen abstraction/acetylene addition revealed. *Angewandte Chemie - International Edition*, 53 (30):7740–7744, 2014. ISSN 15213773. doi:10.1002/anie.201404537.

[37] A. Raj. Structural effects on the growth of large polycyclic aromatic hydrocarbons by C_2H_2. *Combustion and Flame*, 204:331–340, 2019. doi:10.1016/j.combustflame.2019.03.027.

[38] A. Raj, S. Y. Yang, D. Cha, R. Tayouo, and S. H. Chung. Structural effects on the oxidation of soot particles by O_2: Experimental and theoretical study. *Combustion and Flame*, 160(9):1812–1826, 2013. doi:10.1016/j.combustflame.2013.03.010.

[39] H. Sabbah, L. Biennier, S. J. Klippenstein, I. R. Sims, and B. R. Rowe. Exploring the role of pahs in the formation of soot: Pyrene dimerization. *The Journal of Physical Chemistry Letters*, 1(19):2962–2967, 2010. doi:10.1021/jz101033t.

[40] F. Schulz, M. Commodo, K. Kaiser, G. D. Falco, P. Minutolo, G. Meyer, A. D'Anna, and L. Gross. Insights into incipient soot formation by atomic force microscopy. *Proceedings of the Combustion Institute*, 37(1):885 – 892, 2019. ISSN 1540-7489. doi:https://doi.org/10.1016/j.proci.2018.06.100.

[41] T. Stuyver, B. Chen, T. Zeng, P. Geerlings, F. De Proft, and R. Hoffmann. Do diradicals behave like radicals? *Chemical reviews*, 119(21):11291–11351, 2019. doi:10.1021/acs.chemrev.9b00260.

[42] D. W. Szczepanik, M. Solà, T. M. Krygowski, H. Szatylowicz, M. Andrzejak, B. Pawełek, J. Dominikowska, M. Kukułka, and K. Dyduch. Aromaticity of acenes: the model of migrating π-circuits. *Physical Chemistry Chemical Physics*, 20(19): 13430–13436, 2018. doi:10.1039/C8CP01108G.

[43] L. M. Thompson and H. P. Hratchian. Spin projection with double hybrid density functional theory. *The Journal of Chemical Physics*, 141(3):034108, 2014.

[44] T. Totton, A. Misquitta, and M. Kraft. A quantitative study of the clustering of polycyclic aromatic hydrocarbons at high temperatures. *Phys. Chem. Chem. Phys.*, 14(12):4081, 2012. doi:10.1039/c2cp23008a.

[45] T. S. Totton, A. J. Misquitta, and M. Kraft. Assessing the Polycyclic Aromatic Hydrocarbon Anisotropic Potential with Application to the Exfoliation Energy of Graphite. *The Journal of Physical Chemistry A*, 115(46):13684–13693, 2011. doi:10.1021/jp208088s.

[46] R. S. Tranter, S. J. Klippenstein, L. B. Harding, B. R. Giri, X. Yang, and J. H. Kiefer. Experimental and theoretical investigation of the self-reaction of phenyl radicals. *The Journal of Physical Chemistry A*, 114(32):8240–8261, 2010. doi:10.1021/jp1031064.

[47] A. Veshkini, N. A. Eaves, S. B. Dworkin, and M. J. Thomson. Application of pah-condensation reversibility in modeling soot growth in laminar premixed and nonpremixed flames. *Combustion and Flame*, 167:335–352, 2016. doi:10.1016/j.combustflame.2016.02.024.

[48] A. Violi, A. Kubota, T. Truong, W. Pitz, C. Westbrook, and A. Sarofim. A fully integrated kinetic monte carlo/molecular dynamics approach for the simulation of soot precursor growth. *Proceedings of the Combustion Institute*, 29(2):2343–2349, 2002. doi:10.1016/S1540-7489(02)80285-1.

[49] H. Wang. Formation of nascent soot and other condensed-phase materials in flames. *Proceedings of the Combustion Institute*, 33(1):41–67, 2011. doi:10.1016/j.proci.2010.09.009.

[50] R. Whitesides, D. Domin, R. Salomón-Ferrer, W. A. Lester, and M. Frenklach. Embedded-ring migration on graphene zigzag edge. *Proceedings of the Combustion Institute*, 32 I(1):577–583, 2009. doi:10.1016/j.proci.2008.06.096.

[51] H.-B. Zhang, X. You, H. Wang, and C. K. Law. Dimerization of polycyclic aromatic hydrocarbons in soot nucleation. *The Journal of Physical Chemistry A*, 118(8): 1287–1292, 2014. doi:10.1021/jp411806q.

[52] Y. Zhao and D. G. Truhlar. The M06 suite of density functionals for main group thermochemistry, thermochemical kinetics, noncovalent interactions, excited states, and transition elements: two new functionals and systematic testing of four M06-class functionals and 12 other functionals. *Theoretical Chemistry Accounts*, 120 (1-3):215–241, 2008. doi:10.1007/s00214-007-0310-x.